ACS Catalysis

Research Article

pubs.acs.org/acscatalysis

Characterization of Coke on a Pt-Re/γ-Al_2O_3 Re-Forming Catalyst: Experimental and Theoretical Study

Simon R. Bare,*[,†] F. D. Vila,[‡] Meghan E. Charochak,[§] Sesh Prabhakar,[§] William J. Bradley,[∥] Cherno Jaye,[⊥] Daniel A. Fischer,[⊥] S. T. Hayashi,[‡] Steven A. Bradley,[§] and J. J. Rehr[‡]

[†]SSRL, SLAC National Accelerator Laboratory, Menlo Park, California 94025, United States

[‡]Department of Physics, University of Washington, Seattle, Washington 98195, United States

[§]Honeywell UOP, Des Plaines, Illinois 60017, United States

[∥]Department of Chemistry, Iowa State University, Ames, Iowa 50011, United States

[⊥]Materials Measurement Laboratory, National Institute of Standards and Technology, Gaithersburg, Maryland 20899, United States

Supporting Information

ABSTRACT: The characterization of coke on spent catalysts is key to understanding deactivation mechanisms in hydrocarbon transformations. In this paper we report the comprehensive characterization (using laser Raman spectroscopy, ^{13}C MAS NMR, temperature-programmed oxidation, XPS, and carbon K-edge NEXAFS) of coke on a series of spent Pt-Re re-forming catalysts as a function of time on stream and position in the catalytic bed. Laser Raman spectroscopy is shown to be rather insensitive to the carbon species present, while ^{13}C MAS NMR finds that the carbon is present primarily as aromatic carbon. The TPO data are consistent with the coke being present on the alumina support and not to a large extent covering the metallic Pt-Re nanoclusters, but the data do suggest the presence of more than one type of coke present. The carbon K-edge NEXAFS data, however, clearly differentiate the types of coke species present. In the more coked samples the features ascribed to graphite become more pronounced, together with an increase in the aromaticity, as judged by the intensity of the π^* peak. With increasing amounts of carbon on the catalyst there is also a concomitant decrease in the σ^* C−H peak, indicating that the carbon is becoming less hydrogenated. By using a linear combination of C NEXAFS spectra for *n*-hexane, benzene, and broadened highly oriented pyrolytic graphite (HOPG), we estimate the compositional change on the coke species, verifying the aliphatic to aromatic conversion. The data indicate that a good model for the deposited coke is that of highly defected, medium-sized rafts with a short-range polycyclic aromatic structure which have a variety of points of contact with the alumina surface, in particular with the O atoms. In agreement with the NMR, there is evidence for the C−O functionality from the presence of a shoulder in the C NEXAFS spectra that is ascribed, as a result of DFT calculations, to a 1s → π^* transition of the carbon atoms bound to the oxygen of a phenoxide-like species bound to the alumina surface. These data confirm earlier Soxhlet extraction studies and show that extraction process did not substantially change the character of the coke from what it was while still in contact with the catalyst surface.

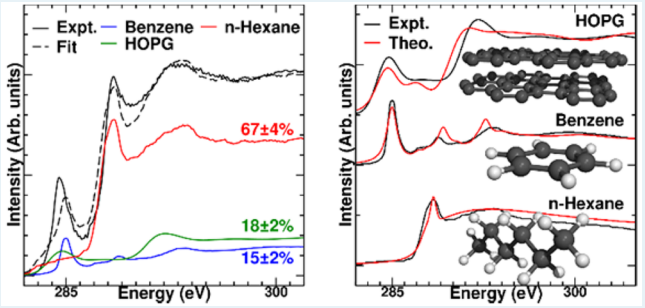

KEYWORDS: *carbon NEXAFS, coke characterization, catalyst deactivation, Pt-Re/alumina, TPO, DFT calculations, ^{13}C MAS NMR, Raman*

INTRODUCTION

The characterization of coke on spent catalysts has been of longstanding interest primarily due to the fact that coke deposition typically results in deactivation of the catalyst, thereby shortening its useful life, and also because it can provide insight into the reaction mechanism.[1] Some of the typical characterization methods employed to study the carbon on spent catalysts are laser Raman spectroscopy,[2−5] temperature-programmed oxidation (TPO),[6−10] including the work of Perera and colleagues,[6,11,12] ^{13}C CP MAS NMR,[7,9] and X-ray spectroscopy, as discussed below.

A classical method of characterizing the coke on spent catalysts is to use Soxhlet extraction in methylene chloride to separate the soluble (soft) and insoluble coke (hard) fractions.[13] In this process soft coke extractions are distilled to remove the solvent and analyzed by HPLC, GC, or MS, for example.[14] The solid portion of the sample, containing the remaining insoluble carbon, is dried and the carbon is analyzed (either with the catalyst or by demineralization to obtain only

Received: September 29, 2016
Revised: December 30, 2016
Published: January 9, 2017

DOI: 10.1021/acscatal.6b02785
ACS Catal. 2017, 7, 1452−1461

the coke portion) by various techniques such as TGA, IR, Raman, NMR, and microscopy. Alternatively, Soxhlet extraction may be carried out in different solvents (e.g., hexane, chloroform, and toluene) in order to identify the degree of hydrogenation of coke species in soluble form.[15] It has been shown that the extraction procedure does not modify the nature of the coke or generate any new carbon species.[16] However, it is debatable whether this is true for every catalyst system.[17] It has been demonstrated that aliphatic coke can be extracted by Soxhlet extraction and that the insoluble coke is highly aromatic, which increases with reaction temperature and time on stream.[17] However, one of the questions with such an extraction procedure is whether the extraction process substantially changes the character of the coke from what it was while still in contact with the catalyst surface. This work, therefore, seeks to address this question by focusing on a novel and different approach: namely, the interaction of coke on the actual catalyst surface. All of the anisotropic interactions of coke with the solid surface will be lost in the extracted material. More recently, with the advent of aberration corrected transmission electron microscopes, it has been possible to study the location of the carbon relative to the dispersed metal nanoclusters on a Pt-Re re-forming catalyst, leading to a new understanding of the mechanisms of coke deposition.[18] However, what is still lacking is a comprehensive and detailed understanding of the nature of coke that is deposited under realistic pilot plant conditions using a formulated re-forming catalyst.

A technique that shows promise for a detailed characterization of coke on catalysts is carbon K-edge near-edge X-ray absorption fine structure (NEXAFS) spectroscopy. It is element specific, has the ability to differentiate the local chemistry of the carbon, can be conducted (pseudo) in situ, and can be applied to technical catalysts. However, to date there have only been a few reported instances of its use to study the types of carbon on actual formulated spent catalysts.[19−22] In contrast, there are many examples of the use of carbon NEXAFS to probe adsorbed hydrocarbons on model catalysts.[23−25] It is likely that part of the reason for the dearth of studies is that there are only a few beamlines at light sources where these data could be collected, in combination with the difficulty of making the measurements from nonplanar catalysts. Moreover, a detailed interpretation of the C NEXAFS spectra is also not straightforward, requiring parallel theoretical studies for quantitative characterizations.

The work of Shimada et al. highlighted that C NEXAFS could be used to distinguish the coke formed on fluid catalytic cracking (FCC) catalysts, hydrotreating catalysts, and catalysts used for the dry re-forming of methane,[21,22] while the earlier work of Davis et al. reported on the use of carbon NEXAFS to study the gas oil derived coke deposits on a LZ-210 zeolite.[20] However, missing from the earlier work is a link back to more traditional methods of coke characterization, combined with an assignment of the peaks in the C NEXAFS spectra based on accurate theoretical calculations. Consequently, we have undertaken such a study with the aim of applying C NEXAFS as a characterization technique for spent catalysts of industrial importance (hydrocarbon re-forming catalysts), providing a sound theoretical basis for the interpretation of the NEXAFS spectra, and combining this information with that obtained from laser Raman spectroscopy, XPS, temperature-programmed oxidation, and ^{13}C NMR. Each of these techniques provides useful information, but it is only with their combined information that a more complete understanding of the deposited carbon on the catalyst is obtained. The catalysts in this study were generated in a pilot plant using relevant re-forming conditions.[18] This series of catalysts provided a set of samples containing different levels of coke that had all been generated in the same pilot plant under the same reaction conditions.

EXPERIMENTAL METHODS

Catalyst Preparation and Testing. The Pt-Re/γ-Al_2O_3 catalyst was prepared and tested as previously described.[18] Briefly, the catalyst was prepared as a 1.3:1 (Pt:Re) ratio impregnated on 1.6 mm diameter γ-Al_2O_3 extrudates. After impregnation the catalyst was calcined at 510 °C and then reduced at 510 °C in 15 mol % hydrogen for 2 h. The pilot plant testing was conducted at a total pressure of 200 psig by cofeeding 1.5 mol of H_2 with 1 mol of naphtha, which can be characterized as a mixture of about 60% aliphatic (25% *n*-hexane, 10% pentane, 10% heptane, 15% cyclohexane) and 40% aromatic (25% xylene, 15% toluene) compounds. The hydrocarbon feed had an initial boiling point of 79 °C and an end boiling point of 166 °C. The catalyst was tested for varying amounts of time (10 and 96 h), and the bed was portioned into top, middle, and bottom of the bed after testing.

Compositional Analysis. The metal loading on the catalyst was determined using inductively coupled plasma (ICP). The concentration of carbon on the spent samples was determined using a LECO Corporation CS600-series combustion analyzer equipped with an infrared spectrometer.

Laser Raman Spectroscopy. Laser Raman spectra were measured from as-received powders contained in thin-walled (10 μm) quartz capillaries rotated at 1000 rpm. The spectra were acquired in backscatter configuration using a Kaiser Holoprobe Raman spectrometer with the red laser (785 nm, 45 mW, 5× magnification), and 90 s detector exposure time per spectrum. The spectra were processed using GRAMS/AI 9.1 software and truncated between 1800 and 300 cm^{-1} with baseline correction.

Carbon NEXAFS. The carbon NEXAFS data were collected from the parallel processing imaging system at beamline U7A at the National Synchrotron Light Source (NSLS) at Brookhaven National Laboratory. The partial electron yield (PEY) spectra were obtained using a channeltron electron multiplier with an adjustable entrance grid bias (EGB). A negative bias of 50 V was applied to reject extraneous background due to low-energy electrons. Data were recorded in a UHV chamber, at room temperature, with an incident X-ray resolution of 0.1 eV. The monochromator energy was calibrated using the carbon K-edge π^* transition of graphite, located at 285.35 eV. To eliminate the effect of fluctuations in the incident beam intensity and of monochromator absorption features, the PEY signals were normalized using the incident beam intensity obtained from the photoemission yield of a clean Au slit frame located upstream along the path of the incident X-ray beam. The samples were positioned at an angle of 55° relative to the incident beam. The spectra were processed through standard pre- and postedge normalization methods. Details can be found in previously published work.[26,27]

X-ray Photoelectron Spectroscopy. The XPS spectra were collected using monochromatic aluminum Kα radiation (1486.6 eV) with a Physical Electronics Quantera X-ray photoelectron spectrometer. The base pressure was kept at ~1×10^{-9} mbar. Charging was neutralized using the combined

DOI: 10.1021/acscatal.6b02785
ACS Catal. 2017, 7, 1452−1461

low-energy electron flood gun and low-energy argon ion gun of the instrument. Survey scans were collected using a pass energy of 224 eV and region scans with a pass energy of 69 eV. The data were collected from ground powder pressed into a molybdenum sample holder. The spectra were acquired using an X-ray power setting of 80 W, with a 100 μm diameter X-ray beam diameter rastered over a 1400 μm × 200 μm area per sample. The surface elemental concentrations were calculated using the integrated peak areas of the appropriate peaks making use of integrated Physical Electronics data analysis software (Multipak).

Temperature-Programmed Oxidation. The TPO data were acquired using a TA Instruments Q5000 IR TGA apparatus. The sample was ramped at 5 °C/min under a flow of 1% O_2 in nitrogen to a final temperature of 650 °C.

Solid State ^{13}C NMR. The ^{13}C CP MAS NMR data were collected using a Bruker Avance-200 spectrometer operating at a carbon frequency of 50.3096 MHz (the corresponding proton frequency is 200.0569 MHz). All CP MAS experiments were carried out using 7 mm rotors spinning at 5 kHz. A 6.8 μs proton pulse and a contact time of 3 ms were employed. The number of accumulations ranged from 64k to 262k depending on the carbon levels present in the samples. The delay between each acquisition was set to 1 s. The catalyst extrudates were placed in the rotor, crushed to a powder, and packed. The CP conditions were established using a standard sample of glycine, and the same conditions were used for recording the spectra of the catalyst samples. The peak positions were reported with respect to TMS, which was set to 0 ppm. Total suppression of spinning sidebands (CP-TOSS) was employed to check for any spinning sidebands overlapping with the isotropic peaks. Cross-polarization NMR intensities are very sensitive to the size of the dipolar couplings, concentration and relaxation behavior of the respective nuclei involved, number of protons attached to carbon, and experimental parameters such as matching conditions, spinning speed, contact times, etc. Molecular motion and the presence of stable free radicals also affect accurate quantitation of carbon intensities.[28] Hence, the results reported should be considered semiquantitative. It was reported that accurate relative signal intensities for various organic functional groups are possible with a contact time of around 3 ms.[29]

StoBe DFT Calculations. All C K-edge XANES simulations reported here were performed using the StoBe-deMon code[30] with the Slater transition potential approach.[31] In this single-particle approximation, the absorption intensity I is calculated using Fermi's golden rule

$$I \propto \frac{1}{\omega} \sum_i |\langle c|\hat{e}\cdot\vec{r}|i\rangle|^2 \times \delta(\omega + E_i - E_c)$$

where ω is the photon energy, $\hat{e}$ is the light polarization vector, and c and i indicate the initial core and final states, respectively, computed in the presence of a half-occupied core state. Given the presence of this half-occupied core state, the basis set must be carefully chosen to accurately describe the electron density relaxation around the absorbing atom. For this purpose, the basis set used for the absorber was an all-electron, fully uncontracted IGLO III[32] supplemented with (5,2;5,2) auxiliary basis functions. The nonabsorbing C, Al, and O atoms used (3,1:8,0), (4:6,4), and (3,1:10) effective core potentials, (321/311/1), (311/31/1), and (321/311/1) basis sets, and (5,2;5,2), (3,3;3,3), and (5,2;5,2) auxiliary basis functions, respectively. Finally, all H atoms used the all-electron 6-311G basis set. All XANES simulations used the BP86[33,34] gradient-corrected exchange-correlation functional. When available, experimental structures were used in the calculations. Otherwise, they were either taken from the NIST structure database[35] or, in the case of aluminum phenoxide, obtained by optimizing an isolated molecule in the gas phase using the Gaussian code with the B3LYP functional[36,37] and a 6-31+G(d,p) basis set. To simulate highly oriented pyrolytic graphite (HOPG), a cluster model based on the experimental structure of graphite was built, with a central layer of six fused rings, and the above and below layers were simulated by a single benzene ring above the absorbing atom. Given that the molecules studied have a variety of symmetry-unique C atoms, we carried out separate calculations with the core-hole on each and averaged the results (with the exception of HOPG, where a single representative atom was used). Before averaging and to facilitate comparison with experiment, each individual spectrum was broadened using an ad hoc self-energy. Although the experimental signal results from a superposition of spectra from several types of carbon atoms, we have attempted to fit it using a linear combination of three principal components: benzene, broadened HOPG, and *n*-hexane. Benzene and HOPG are representative of sp^2-bonded C atoms, while *n*-hexane represents the sp^3-bonded C atoms in the system. These three compounds exhibit distinctly different X-ray spectra, due to the different local densities of states around the absorbing atoms. For example, the planar sp^2 hybridization of the aromatic atoms shows a distinct π^* resonance that is not present in the fully coordinated sp^3 atoms. As a basis for the fits we used both experimentally measured spectra (benzene taken from ref 38, *n*-hexane from ref 39, and HOPG measured in this work) and theoretical spectra computed with the DFT methodology described above. The experimental HOPG spectrum was broadened by 0.8 eV to account for disorder in the coke, as described in the discussion below. The fits to experiment were performed using the Athena code, using the standard pre- and postedge normalized spectra.[40] These fits minimize the reduced $\bar{\chi}^2$ value (i.e., the ratio of the mean-squared error in the fit to the mean-square error in the data) defined as $\bar{\chi}^2 = 1/(N\varepsilon^2)\sum_i^N (y_i^{\mathrm{exp}} - y_i^{\mathrm{fit}})^2$, as a function of the weights of the three basis components. Here N is the number of points fitted (~1000) and ε is an estimate of the experimental error estimated by fitting a smooth polynomial to the upper region of the spectra ($\varepsilon \cong 0.0045$). The errors in the weights were obtained by adding 10% artificial random noise to the experimental signal and computing the mean variation of the weights at that level of noise.

RESULTS AND DISCUSSION

The weight loading of the catalyst was determined to be 0.35 wt % Pt and 0.25 wt % Re. Table 1 summarizes the amount of carbon on each of the spent catalyst samples after the pilot plant testing (determined using the LECO CS600 instrument), together with the designation (e.g., 10HT) used for each sample throughout the paper. The increasing amount of carbon in the samples is consistent with an increasing amount of olefinic coke precursors down the catalyst bed in the down flow reactor.

The laser Raman spectra of the samples are shown in Figure 1.

With the exception of the spectrum from 10HT, the spectra of all of the spent catalysts are similar. There is a narrow peak

DOI: 10.1021/acscatal.6b02785
ACS Catal. 2017, 7, 1452−1461

Table 1. Weight Percent of Carbon and the Designations Used throughout the Paper for the Six Spent Catalysts

sample	designation	carbon (wt %)
10 h top of bed	10HT	0.6
10 h middle of bed	10HM	2.4
10 h bottom of bed	10HB	3.6
96 h top of bed	96HT	2.9
96 h middle of bed	96HM	8.2
96 h bottom of bed	96HB	10.6

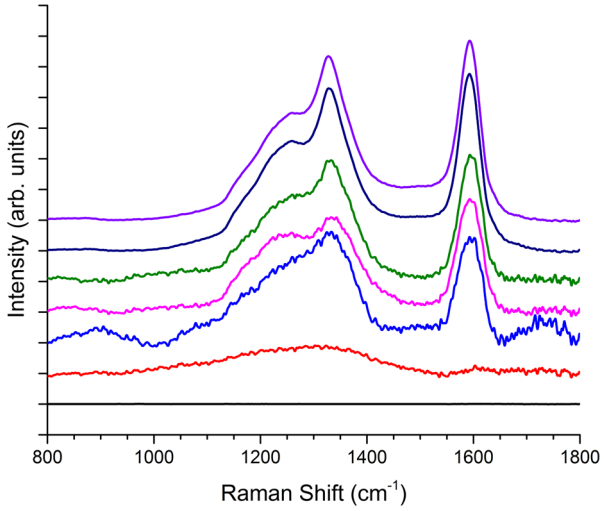

Figure 1. Laser Raman spectra from the spent catalysts, offset for clarity. From bottom to top: 10HT (red), 10HM (blue), 10HB (magenta), 96HT (green), 96HM (black), and 96HB (purple).

centered at 1592 cm^{-1}, a broader peak at 1330 cm^{-1}, and a shoulder peak centered at 1260 cm^{-1}. The definition of the last shoulder becomes more pronounced with increasing amounts of carbon on the samples. There is no measurable shift in any of the peak maxima as a function of time on stream or position in the catalyst bed. The 10HT spectrum shows only a broad peak centered at around 1300 cm^{-1}. The overall relative intensities of the peaks are similar for all of the samples (except 10HT) as are the ratios of the intensities of the 1592 and 1330 cm^{-1} peaks, which are close to unity. The band around 1590 cm^{-1} is traditionally assigned as the G band, while that at around 1370 cm^{-1} is the D band. These names arise from the former being the only allowed peak in Raman for pure graphite (G), while the latter is due to disorder (D) in the graphitic structure. In pure graphite the G peak is narrow, and the broadness of the peaks in this study can be related to the degree of disorder/inhomogeneity in the deposited coke on the catalyst.[3] Moreover, it has been shown that ratio of the intensity of the D band to the G band depends inversely on the size of the graphite microcrystals in the sample.[41,42] From the data in Figure 1, the relative intensities of the two bands for all of the spent catalysts are approximately unity, which indicates a crystallite size of around 30 Å. It is noted that the inferred size of the crystallites does not change with increased deposition of carbon on the samples. In addition to the G and D bands, there is also a prominent shoulder at ~1260 cm^{-1}. The definitive assignment of this peak is elusive. It has been observed previously on (i) aged hydrotreating catalysts, where it was assigned to C−H vibrations,[2] (ii) coked reforming catalysts, where it was not assigned but was most prominent on catalysts containing only chlorided alumina and thus could be more indicative of coke on the alumina support as opposed to on the metal nanoparticles,[4] and (iii) on coked ZSM-5 and USY zeolites, where the peak was not assigned.[5] It is likely that this peak is related to the presence of hydrogenated coke and is due to a C−H deformation mode.

XPS was used to estimate the amount of coke present on the spent catalyst surface, and this was compared to the bulk weight percent of carbon. Figure S1 in the Supporting Information suggests that there is a linear relationship between the C:Al ratio and the amount of carbon deposited on the catalyst. While detailed modeling is needed to conclusively determine the growth mechanism of the carbon on the alumina support, semiquantitatively the data indicate that there is no "bulk" coke deposited on the catalyst; rather, the coke is present either as a thin layer on the alumina surface or as an expanding island morphology. This inference is in agreement with a prior STEM study[18] and with prior work on commercial spent Pt-Re/γ-Al_2O_3 catalysts, where it was concluded that the coke was present in a 1 nm constant-thickness layer.[43]

TPO data were collected on all of the catalysts in order to provide information related to the ease of removal of the coke by combustion. The resulting first derivatives of the weight loss with respect to temperature for each of the spent catalysts are plotted in Figure 2. Prior to the major weight loss at >400 °C,

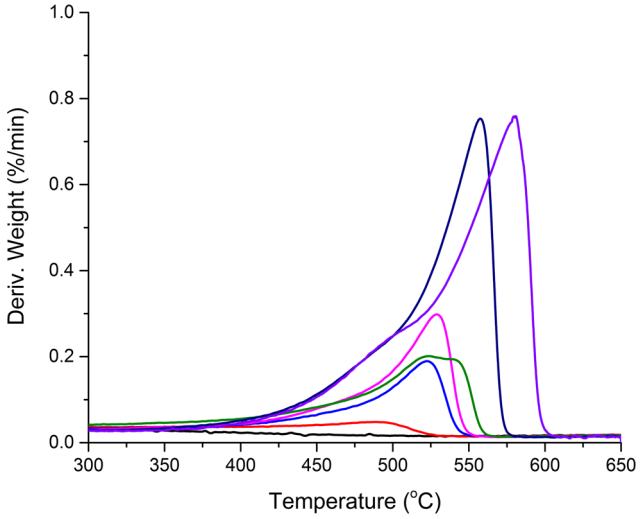

Figure 2. First derivative of the TPO curves for the six spent catalysts: fresh (black), 10HT (red), 10HM (blue), 10HB (magenta), 96HT (green), 96HM (black), and 96HB (purple).

assigned to the combustion of the coke (and depicted in Figure 2), there is a weight loss in the temperature range up to 200 °C primarily due to removal of physisorbed water and other volatile compounds. The raw TPO curves for the fresh catalyst and the 96HB sample are shown in Figure S2 in the Supporting Information. As can be seen in Figure 2, there are three distinct peaks, as determined from the temperature of the maximum in the rate of weight loss during the TPO, curves suggesting that there are three types of coke on the spent catalysts. The 10HT sample has a peak maximum at around 495 °C which shifts to 525 °C in the 10HB sample. The 96H samples show different behavior. The 96HT sample appears to show the same peak as the 10H samples but also has an additional peak at 540 °C. This peak appears to shift to 550 °C in the 96HM sample, and finally the peak is shifted to 580 °C in the 96HB sample. The

DOI: 10.1021/acscatal.6b02785
ACS Catal. 2017, 7, 1452−1461

integrated area of the TPO rate curves as a function of the bulk weight percent of carbon on the samples is displayed in Figure 3. The integrated area is effectively the amount of carbon

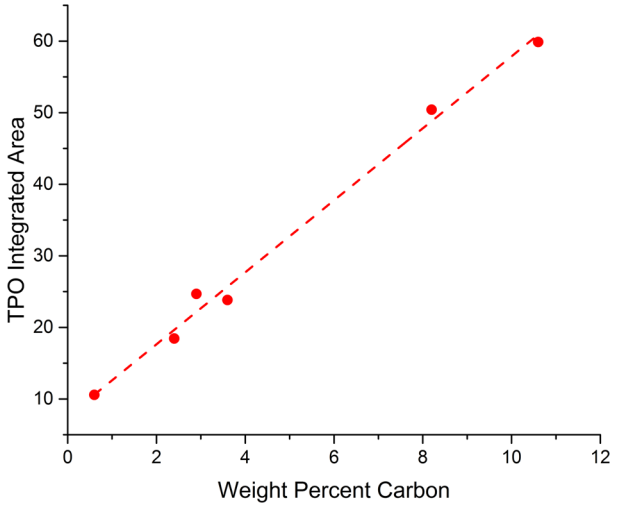

Figure 3. Integrated area of the TPO curves (determined using the TA Q5000 instrument) as a function of the weight percent of carbon on the spent catalysts (determined using the LECO CS600 instrument).

dioxide generated during the coke combustion. As can be seen, there is a linear relationship between the amounts of carbon on the catalyst as the TPO area. Coke deposited on the metals (Pt and Re in this case) is oxidized at low temperature, between 200 and 400 °C, whereas coke deposited on the alumina is oxidized at higher temperature, typically >500 °C (ref 8 and references therein). The data in Figure 2 indicate that there is little, if any, coke deposited on the Pt-Re clusters on the catalyst. This conclusion is in agreement with the prior STEM characterization of the 10HB and 96HB samples, which showed the coke to be present primarily on the alumina support.[18] An important observation in the STEM study was that in the early stages of coking the carbon is relatively homogeneously dispersed across the catalyst, with no distinguishable features, whereas with the high level of coke on the 96HB sample the carbon is now heterogeneously distributed with regions rich in coke adjacent to regions with significantly lower levels of coke. The greater amount of coke thus would require a higher temperature or longer time to combust. It has also been reported that a shift to higher temperature in TPO is an indication of the increasing degree of graphitization of the coke.[44]

The ^{13}C CP MAS NMR data are summarized in Table 2, and the spectra are shown in Figure S3 in the Supporting Information. Only the samples from the top of the bed, 10HT and 96HT, show measurable carbon species other than aromatic carbon. The peak position of the aromatic carbon corresponds to protonated and internal carbon of polynulcear aromatics. In addition, the sample with the least amount of carbon, 10HT, also shows a peak assigned to oxygen functionalized carbon, either C═O or C−O. The aliphatic peak position corresponds to methyl groups attached to aromatic rings. The fact that the 10HT sample with very low carbon shows a considerable CP signal indicates the more hydrogenated nature of the coke present. These NMR data, showing that the coke is mostly aliphatic in the early stages and

Table 2. Relative Integrated Intensities of Various Types of Carbons in Spent Catalysts Obtained by ^{13}C CP MAS NMR Spectroscopy

		carbon species (% C)		
sample	designation	aliphatic	aromatic	C═O and C−O
10 h top of bed	10HT	28.9	57.4	13.7
10 h middle of bed	10HM	0	100	0
10 h bottom of bed	10HB	0	100	0
96 h top of bed	96HT	21.6	78.4	0
96 h middle of bed	96HM	0	100	0
96 h bottom of bed	96HB	0	100	0

then becomes mostly aromatic in the later stages, is in agreement with prior work.[13−17]

The carbon NEXAFS of the six spent samples are shown in Figure 4. The spectra show both some similarities and also

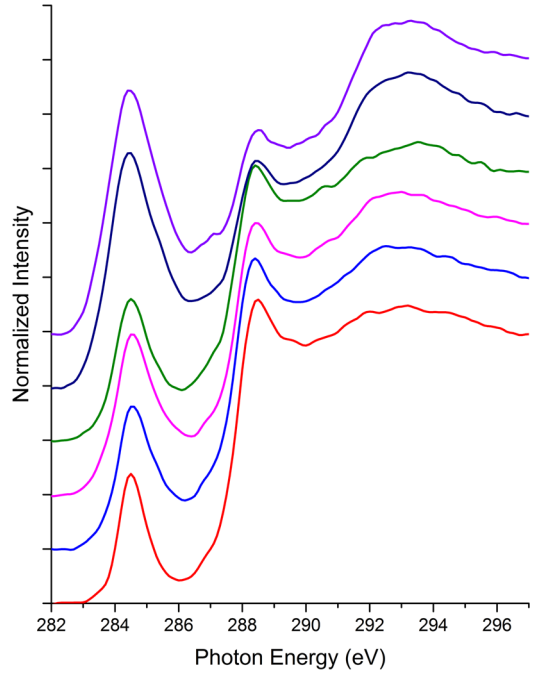

Figure 4. Carbon NEXAFS spectra of the spent catalysts, offset for clarity. From bottom to top: 10HT (red), 10HM (blue), 10HB (magenta), 96HT (green), 96HM (black), and 96HB (purple).

some important differences. There are four distinct features present in the spectra at approximately 284.5, 287, 288.5, and 293 eV. To aid in the discussion of these spectra and the assignment of the spectral features, the C NEXAFS spectra of highly oriented pyrolytic graphite (HOPG) and aluminum phenoxide ($Al(OPh)_3$) are displayed with the spectra of 10HB and 96HB in Figure 5.

Each spectrum shows a relatively sharp resonance at 285.3 eV which is assigned to the transition to π^* antibonding orbitals of aromatic/olefinic hydrocarbons, the so-called π^* resonance. This resonance is associated with C atoms with a planar or quasi-planar local environment and sp^2 hybridization. The relative intensity of this peak grows with an increasing amount of carbon on the catalyst, suggesting that the carbon becomes more unsaturated/aromatic. The broad resonance centered at approximately 293 eV is the σ^*(C−C) transition.[23,45] This peak becomes more distinct with a well-

DOI: 10.1021/acscatal.6b02785
ACS Catal. 2017, 7, 1452−1461

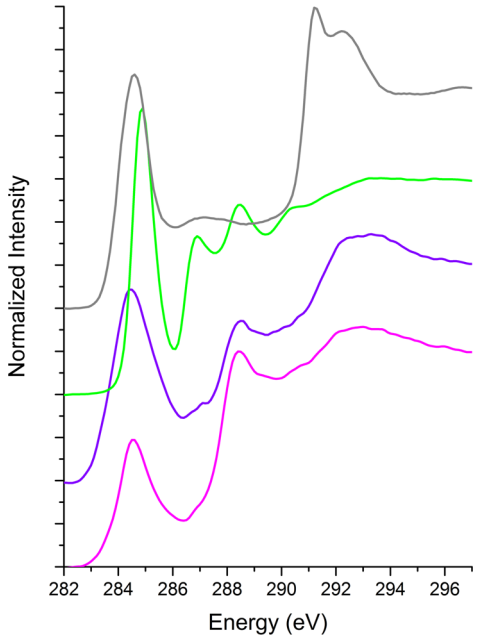

Figure 5. Carbon NEXAFS spectra of two of the catalysts together with those of reference compounds. From bottom to top: 10HB (magenta), 96HB (purple), aluminum phenoxide (green), and HOPG (black).

defined rising edge at 291.5 eV in the 96HM and 96HB samples and now resembles that of the C NEXAFS spectrum of HOPG (Figure 5). This peak is known to be sensitive to the structural and electronic structure of the graphite,[46] and the fact that it is only defined in the 96HM and 96HB samples suggests that the short-range graphitic nature of the coke is more well developed in these samples: i.e., that the thin layers of graphite we believe form most of the coke are becoming bigger, less defected, or a combination of both. The peak at 288.5 eV is assigned to a C−H σ^* resonance.[23,45,47] At low levels of carbon in the 10H samples, the relative intensity of this peak is larger than that from those with increased levels of carbon (96H samples). Thus, with increased aromaticity of the carbon there is a corresponding decrease in the proportion of hydrogenated carbon.[14−17] The small shoulder at 287 eV is not as straightforward to assign, but it is noted that the C NEXAFS spectrum of aluminum phenoxide has a distinct peak at this energy (Figure 5). The assignment of this peak is discussed further below.

Additional insight regarding the nature of the coke deposited on the spent re-forming catalysts can be gained by further analyzing the C NEXAFS spectra.

First, plotted on Figure 6A is the step height of the carbon NEXAFS versus the bulk weight percent of carbon on the catalysts. The step height is determined using accepted methods[48] and is illustrated in Figure S4 in the Supporting Information. There is an approximately linear relationship between these variables, indicating that the magnitude of the absorption edge can be used as a measure of the amount of carbon on the catalyst. Second, Figure 6B shows the relative intensity of the σ^* C−H peak relative to the amount of carbon on the sample (step height) versus the wt % carbon on the sample. As can be seen the relative intensity of the σ^* C−H peak decreases with increasing coke on the catalyst indicating that the coke becomes less hydrogenated as a function of time on stream. This observation is in agreement with the ^{13}C CP

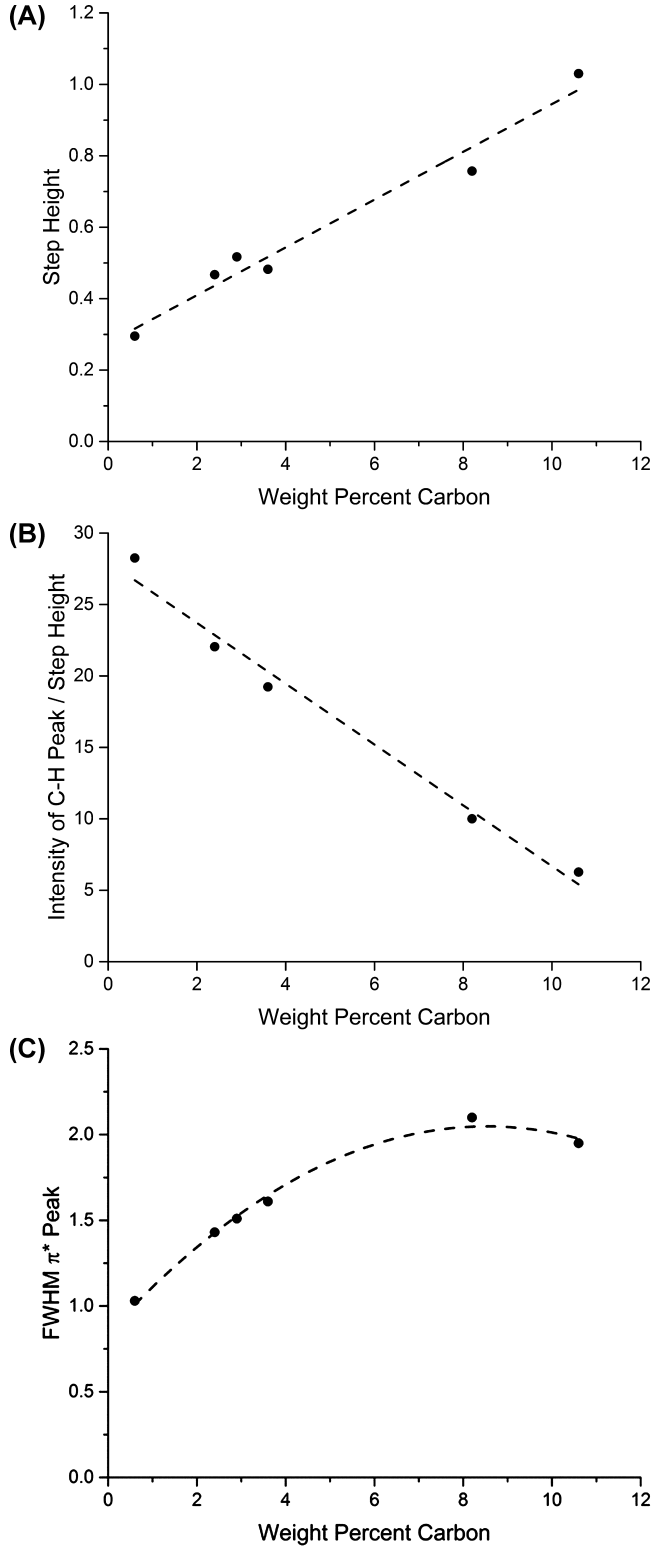

Figure 6. (A) Step height of the carbon NEXAFS spectra of the spent catalysts versus the weight percent of carbon in the catalysts. (B) Intensity of the C−H peak normalized to the step height versus the weight percent of carbon in the catalysts. (C) fwhm of the π^* peak versus the carbon in the catalysts (C).

MAS NMR data. Finally, Figure 6C plots the full-width at half-maximum (fwhm) of the π^* peak versus the weight percent of carbon on the samples. The fwhm of the π^* peak increases with increasing amount of carbon on the sample from 1 eV to

DOI: 10.1021/acscatal.6b02785
ACS Catal. 2017, 7, 1452−1461

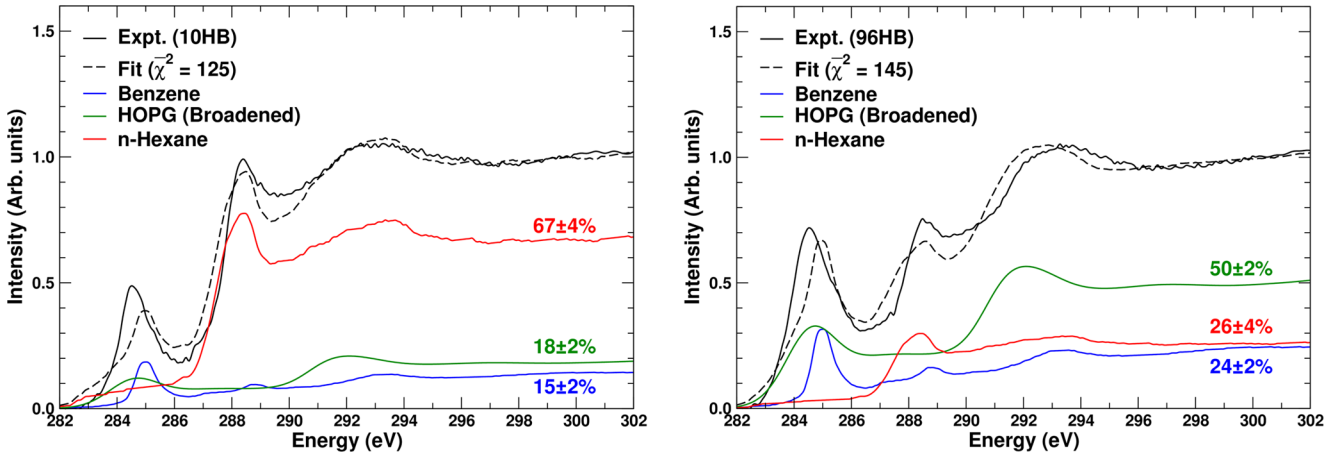

Figure 7. Theoretical fit to the experimental data using experimental *n*-hexane, benzene, and HOPG (broadened by 0.8 eV) spectra as representative of sp^3 and sp^2 C absorbers for the 10HB sample (left) and 96HB sample (right).

around 2 eV fwhm at 8 wt % coke and then levels off. There are several reasons that would lead to changes in the line width and intensity of the π^* peak, including the domain size of the graphitic carbon, the presence of several different peaks at slightly different energies due to different carbon functionalities, and the degree of hydrogenation of the carbon.[47,49−51] It has also been shown that the fwhm of the π^* peak can be used as a measure of the amount of isolated double bonds versus aromatic sextets in the hydrocarbon.[52] The concept of the aromatic sextet-isolated double-bond description of polynuclear aromatic hydrocarbons (PAH) was first introduced by Clar and is often referred to as Clar's model.[53,54] In this description no two aryl rings sharing a hexagon's side can both be aromatic sextets. Bergmann and Mullins showed that there was a linear relationship between the fwhm of the π^* resonance and the carbon atom ratio of the isolated double bonds versus sextets in a series of PAH compounds.[52] If we use their correlation here (Figure 5.5 in their manuscript), then an increase in the fwhm from around 1.5 to 2.0 eV would imply a change in the ratio from approximately 0.4 to about 0.8. This interpretation is not consistent with the ^{13}C CP MAS NMR data. Alternatively, we propose that at least some of the broadening in the π^* peak is due to the interaction of the aromatic rings with the Lewis acid sites on the alumina surface.

In order to help understand the changes observed between the 10HB and 96HB samples, and to help interpret the peak assignments, we have performed least-squares fits of the observed C NEXAFS spectra with a simple basis of three components. These components, benzene, HOPG (or HOPG broadened by 0.8 eV), and *n*-hexane, were chosen as representative of the types of C atoms and their local environments present in the coked samples and dominate the contribution to the XANES apart from fine structure from more distant atoms. The choice of benzene and broadened HOPG is not arbitrary: they represent the extremes of the range of possible aromatic compounds present in the coke, according to the experimental results discussed above. We also considered typical amorphous carbon types as possible components, but this resulted in fits with higher $\bar{\chi}^2$ values in comparison to those with the broadened HOPG. As discussed above, the spectra have two main regions of interest: the π^* peak region (~282−287 eV), due exclusively to unsaturated C components that in the naphtha correspond mostly to aromatic compounds, and the σ^* peak region (~287−293 eV), originating from both saturated and unsaturated components. As stated, by comparing the 10HB and 96HB spectra we see that, as the reaction proceeds, there is a transfer of intensity from the σ^* region to the π^* region, and this is in agreement with all the other data that there is conversion of the carbon species from aliphatic/saturated compounds into aromatic/unsaturated species.[14−17] We attempt to verify this hypothesis and to quantify the conversion using a combination of experimental and theoretical spectra. First, we use a simple linear combination of the experimental spectra of benzene, broadened HOPG, and *n*-hexane to demonstrate that the hypothesis is reasonable. Then we compute the theoretical spectra of these components in order to assign the different observed peaks and attempt to provide a purely theoretical fit of the observed NEXAFS spectra.

Figure 7 shows the fits of the 10HB (left) and 96HB (right) spectra using a linear combination of the experimentally measured NEXAFS spectra of benzene, broadened HOPG, and *n*-hexane. As discussed above, the broadened HOPG simulates the disordered nature of the graphite platelets in the coke. This choice resulted in lower $\bar{\chi}^2$ values for the fits, in particular for the 96HB case. The overall agreement is quite good, with $\bar{\chi}^2$ values of 125 and 145 for the 10HB and 96HB samples, respectively, supporting our hypothesis that the difference in the spectra is due to an aliphatic to aromatic shift. At 10HB, the catalyst spectrum is well reproduced by a mixture of 33% unsaturated (15% benzene and 18% HOPG) and 67% saturated carbon (*n*-hexane). At the end of the run (96HB) the amount of unsaturated carbon has increased to 74% (24% benzene and 50% HOPG), while the amount of saturated C drops to 26%. The most noticeable differences between the fits and the data occur in the π^* region. First, the overall fitted spectra are slightly sharper than the experimental data. This is likely due to disorder in the latter that is not present in the basis components or a variation in the composition that is not represented by the three components used in the fits. Second, the π^* peaks in the fits are blue-shifted by about 0.4 eV from the experiment. Our theoretical simulations show that the position of this peak is modified by substituents, the number of fused rings in the unsaturated compounds, and deformations out of the planarity. Therefore, we believe that the coke present in the catalyst might be formed by larger, substituted aromatic compounds which could also be deformed by contact with the alumina. This hypothesis is supported by the fact that we obtain

DOI: 10.1021/acscatal.6b02785
ACS Catal. 2017, 7, 1452−1461

better fits by using a broadened, i.e. disordered, HOPG instead of the ordered experimental spectra.

Table 3 shows that a three-component mixture provides significantly better fits in comparison to those for only two components, in particular for the 96HB sample. In addition, the fit to this sample is also improved by the inclusion of broadening in the HOPG basis spectrum. Figure 8 shows our theoretical simulations of the basis compounds. The overall agreement is good, with reasonably well reproduced peak positions and relative intensities. In the case of benzene, the peaks at 285 and 289 eV correspond to the π^* peaks, which have an approximate 2:1 ratio (see discussion for aluminum phenoxide below). Energies above 291 eV correspond to the σ^* region. HOPG has a similar spectrum, but with a larger split between the π^* and σ^* regions. Our simplified model of HOPG also underestimates the delocalization of the secondary π^* states above 285 eV, resulting in a narrow single peak at 287 eV, and the continuum above 290 eV, which we have supplemented with an ad hoc background as in the case of aluminum phenoxide discussed below. For *n*-hexane the peak at above 288 eV is associated with the C−H σ^* bonds. A fit (Figure S5 in the Supporting Information) using these theoretical simulations results predicts saturated (*n*-hexane) components of 72% and 30% for the 10HB and 96HB samples, respectively, in reasonable agreement with the 67% and 26% predicted by the fits based on the experimental spectra. The theoretical fits underestimate the relative proportion of HOPG/benzene (4%/24% vs 18%/15% with the experimental spectra for 10HB and 30%/40% vs 50%/24% for the 96HB sample). This is probably due to the poorer theoretically predicted spectra for the HOPG component.

Table 3. Fit Quality ($\tilde{\chi}^2$) of the Different Mixtures Used To Simulate the 10HB and 96HB Samples

	mixture		
sample	*n*-hexane + benzene	*n*-hexane + benzene + HOPG	*n*-hexane + benzene + HOPG (broadened, 0.8 eV)
10HB	152	118	125
96HB	338	161	144

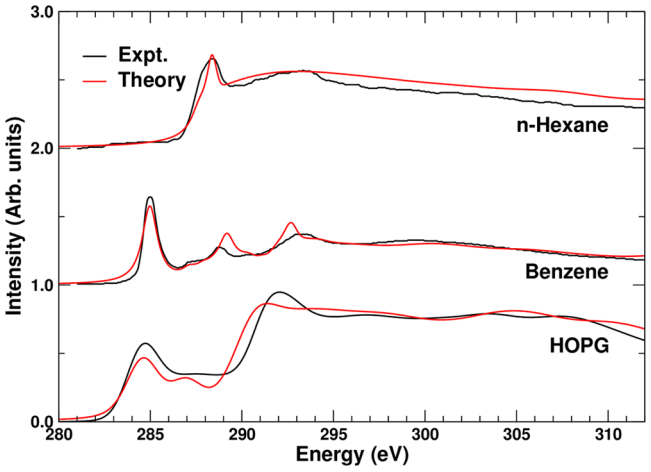

Figure 8. Theoretical simulation of the fit components benzene, HOPG (broadened by 0.8 eV and with a background added above 290 eV), and *n*-hexane.

Finally, we discuss the small shoulder observed at 287 eV. As seen in Figure 9, this peak coincides nicely with a peak observed in the aluminum phenoxide standard. In order to understand the origin of this peak we have calculated the C NEXAFS of aluminum phenoxide and compared it to the experimental data (Figure 9). The good agreement between the calculated and experimental spectra allows for definitive assignment of the peaks. In particular the spectrum is representative of benzene, phenol, and related spectra, as discussed for example by Stohr.[23] The dominant π^* peaks at 285 and 289 eV labeled C_H in Figure 9 exhibit a near 2:1 intensity ratio and a splitting of about 4 eV, as expected for the leading antibonding π^* levels in benzene, and average peak heights of 10/12 and 5/12, respectively. In contrast, the C_O peaks from absorption at the C−O bond at 286 and 291 eV are chemically shifted by about 2 eV, with intensities of about 2/12 and 1/12, respectively. The broader peaks at 295 and 302 eV correspond to broad 1s → σ^* transitions. Beyond the ionization threshold at about 292 eV, one finds a continuum with weak extended fine structure which is reasonably well captured with the extended basis sets.

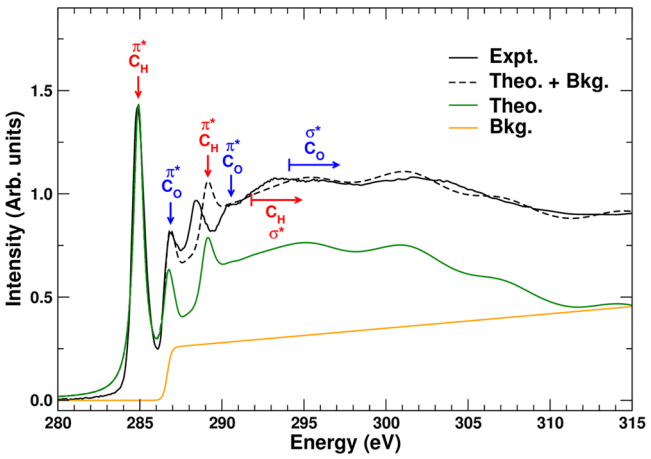

Figure 9. Comparison of the experimental and calculated spectra of aluminum phenoxide. The labels at different energies indicate which carbon atom and type of excitation is responsible for most of the intensity, with C_O corresponding to the carbons bound to the O atom and C_H to those bound to an H atom. The horizontal arrows indicate the onset of the σ^* region for each type of carbon.

Note that the π^* peak is shifted to higher energy in comparison to that of the catalyst data. This shift is expected for a carbonyl-type carbon. The relative intensity of the two transitions is reproduced. These calculations allow the assignment of the small shoulder at 287.0 eV in the spent catalysts (Figure 5) to carbon that is bound to oxygen, which by comparison with the spectrum of the aluminum phenoxide could be an indication of the carbon bound to the alumina surface. Indeed, if the data in Figure 5 are examined carefully, it does appear that the relative contribution of this peak is diminished in the samples with more coke, which would be expected as the amount of carbon increases on the catalyst (less interfacial carbon).

Prior work has shown that the coke formation occurs in a two-stage process.[18] The first stage of the coking involves carbon being deposited uniformly on the catalyst, covering both the Pt-Re nanoparticles and the alumina support. This first stage is accompanied by a sharp drop in activity, with

DOI: 10.1021/acscatal.6b02785
ACS Catal. 2017, 7, 1452−1461

attenuation of all of the active sites. After about 30 h on stream the deactivation of the catalyst stabilizes, and this is accompanied by a steady growth of the coke primarily on the alumina support in a manner that indicates anisotropic growth stemming from the metal nanoparticles. The data presented here now allow us to chemically identify the major form of the coke associated with these two coke regimes. In the first regime, where the activity decreases over the first 20 h on stream, the coke is primarily aliphatic in nature, whereas after extended time on stream the coke converts to primarily a short-range graphitic-type species.

SUMMARY

Characterizing the chemical form of the coke on a spent catalyst and its evolution with time can provide a new understanding that may lead to improvements in the process. The methods highlighted here have all focused on characterizing the carbon while it is present on the catalyst surface and the anisotropic interactions of the carbon with the catalyst surface. The information learned from the different techniques investigated here provide somewhat different views of the types of carbon present on the spent catalysts. Laser Raman spectroscopy is rather insensitive to the carbon species present. With the exception of the 10HT sample, the spectra from the remaining samples are similar and consistent with the presence of a disordered graphitic-type carbon. The ^{13}C NMR is, for the most part, in agreement with this conclusion and the fact that the carbon is present as aromatic carbon. The carbon in the 10HT sample is different from the others and is present as a mixture of aliphatic, aromatic, and C−O functionalized carbon, and for the 96HT sample there is also a significant amount of aliphatic carbon present; however, the Raman spectrum cannot differentiate this. The TPO data are consistent with the coke being present on the alumina support and not to a large extent covering the metallic Pt-Re nanoclusters, but the data do seem to indicate the presence of more than one type of coke present. The C NEXAFS data, however, appear to differentiate the types of coke species present more definitively. In the 96HM and 96HB samples the features ascribed to graphite become more pronounced, together with an increase in the aromaticity, as judged by the intensity of the π^* peak. With an increasing amount of carbon on the catalyst there is also a concomitant decrease in the σ^* C−H peak, indicating that the carbon is becoming less hydrogenated. In agreement with the NMR, there is evidence for a C−O functionality from the presence of a shoulder in the C NEXAFS spectra that is ascribed, as a result of DFT calculations, to a 1s → σ^* transition of the carbon atoms bound to the oxygen of a phenoxide-like species bound to the alumina surface. By using a linear combination of theoretically calculated C NEXAFS spectral data, we have estimated the compositional changes on the coke species. However, even when experimental data are used, the π^* peak position differs by approximately 0.5 eV from that of the unknown coke substance. This is thought to be due to either geometric deformity and/or oxygen bonding. Thus, we believe that a good model for the deposited coke is that of highly defected, medium-sized rafts of carbon with short-range polycyclic aromatic/graphitic structure, which have a variety of points of contact with the alumina surface, in particular with the O atoms.

ASSOCIATED CONTENT

Supporting Information

The Supporting Information is available free of charge on the ACS Publications website at DOI: 10.1021/acscatal.6b02785.

XPS data, weight loss TPO curves, raw NMR spectra, determination of the edge step height from the carbon NEXAFS spectrum, and theoretical fits to the experimental NEXAFS data using theoretically computed *n*-hexane, benzene, and HOPG (PDF)

AUTHOR INFORMATION

Corresponding Author

*E-mail for S.R.B.: simon.bare@slac.stanford.edu.

ORCID

Simon R. Bare: 0000-0002-4932-0342

Notes

The authors declare no competing financial interest.

ACKNOWLEDGMENTS

This research was carried out in part at the National Synchrotron Light Source at Brookhaven National Laboratory, which is supported by the U.S. Department of Energy under Contract No. DE-AC02-98CH10886. F.D.V. and J.J.R. acknowledge partial support of U.S. Department of Energy, Office of Basic Energy Sciences, Catalysis Science Program, Grant No. DE-FG02-03ER15476, with computational support from the NERSC, a DOE Office of Science User Facility, under Contract No. DE-AC02-05CH11231. Norma Kahn is thanked for the XPS data, Randy Zea for the TPO data, and Brendon Lyons for the laser Raman data. Certain commercial names mentioned do not constitute an endorsement by the National Institute of Standards and Technology.

REFERENCES

(1) Bartholomew, C. H. *Appl. Catal., A* **2001**, *212*, 17−60.
(2) Guichard, B.; Roy-Auberger, M.; Devers, E.; Rebours, B.; Quoineaud, A. A.; Digne, M. *Appl. Catal., A* **2009**, *367*, 1−8.
(3) Vogelaar, B. M.; van Langeveld, A. D.; Eijsbouts, S.; Moulijn, J. A. *Fuel* **2007**, *86*, 1122−1129.
(4) Espinat, D.; Dexpert, H.; Freund, E.; Martino, G.; Couzi, M.; Lespade, P.; Cruege, F. *Appl. Catal.* **1985**, *16*, 343−354.
(5) Li, C.; Stair, P. C. *Catal. Today* **1997**, *33*, 353−360.
(6) Parera, J. M.; Figoli, N. S.; Traffano, E. M. *J. Catal.* **1983**, *79*, 481−484.
(7) Sahoo, S. K.; Rao, P. V. C.; Rajeshwer, D.; Krishnamurthy, K. R.; Singh, I. D. *Appl. Catal., A* **2003**, *244*, 311−321.
(8) Barbier, J.; Delmon, B.; Froment, G. F. *Stud. Surf. Sci. Catal.* **1987**, *34*, 1−19.
(9) Martín, N.; Viniegra, M.; Zarate, R.; Espinosa, G.; Batina, N. *Catal. Today* **2005**, *107−108*, 719−725.
(10) Querini, C. A.; Fung, S. C. *Catal. Today* **1997**, *37*, 277−283.
(11) Parera, J. M.; Beltramini, J. N.; Querini, C. A.; Martinelli, E. E.; Churin, E. J.; Aloe, P. E.; Figoli, N. S. *J. Catal.* **1986**, *99*, 39−52.
(12) Pieck, C. L.; Jablonski, E. L.; Parera, J. M.; Frety, R.; Lefebvre, F. *Ind. Eng. Chem. Res.* **1992**, *31*, 1017−1021.
(13) Abdullah, H. A.; Hauser, A.; Ali, F. A.; Al-Adwani, A. *Energy Fuels* **2006**, *20*, 320−323.
(14) Karge, H. G. *Stud. Surf. Sci. Catal.* **1991**, *58*, 531−570.
(15) Afonso, J. C.; Schmal, M.; Frety, R. *Fuel Process. Technol.* **1994**, *41*, 13−25.
(16) Magnoux, P.; Roger, P.; Canaff, C.; Fouche, V.; Gnep, N.; Guisnet, M. *Stud. Surf. Sci. Catal.* **1987**, *34*, 317−330.
(17) Bauer, F.; Karge, H. G. *Mol. Sieves* **2006**, *5*, 249−364.

DOI: 10.1021/acscatal.6b02785
ACS Catal. 2017, 7, 1452−1461

(18) Sanchez, S. I.; Moser, M. D.; Bradley, S. A. *ACS Catal.* **2014**, *4*, 220−228.
(19) Fischer, D. A.; Gland, J. L.; Davis, S. M. *Catal. Lett.* **1990**, *6*, 99−102.
(20) Davis, S. M.; Zhou, Y.; Freeman, M. A.; Fischer, D. A.; Meitzner, G. M.; Gland, J. L. *J. Catal.* **1993**, *139*, 322−325.
(21) Shimada, H.; Imamura, M.; Matsubayashi, N.; Saito, T.; Tanaka, T.; Hayakawa, T.; Kure, S. *Top. Catal.* **2000**, *10*, 265−271.
(22) Shimada, H.; Imamura, M.; Matsubayashi, N.; Sato, T.; Hayakawa, T.; Takehira, K.; Kure, S.; Kinoshita, A.; Nishijima, A. *J. Phys. IV* **1997**, *7*, C2-917−C2-918.
(23) Stöhr, J. *NEXAFS Spectroscopy*; Springer-Verlag: Berlin, Heidelberg, 1992; Vol. *25*.
(24) Fischer, D. A.; Döbler, U.; Arvanitis, D.; Wenzel, L.; Baberschke, K.; Stöhr, J. *Surf. Sci.* **1986**, *177*, 114−120.
(25) Zaera, F.; Fischer, D. A.; Shen, S.; Gland, J. L. *Surf. Sci.* **1988**, *194*, 205−216.
(26) Konicek, A. R.; Jaye, C.; Hamilton, M. A.; Sawyer, W. G.; Fischer, D. A.; Carpick, R. W. *Tribol. Lett.* **2011**, *44*, 99−106.
(27) Baio, J. E.; Jaye, C.; Fischer, D. A.; Weidner, T. *Anal. Chem.* **2013**, *85*, 4307−4310.
(28) Axelson, D. E. *Solid State Nuclear Magnetic Resonance of Fossil Fuels: An Experimental Approach*; Multiscience Publications: London, 1985.
(29) Packer, K. J.; Harris, R. K.; Kenwright, A. M.; Snape, C. E. *Fuel* **1983**, *62*, 999−1002.
(30) Hermann, K.; Pettersson, L. G. M.; Casida, M. E.; Daul, C.; Goursot, A.; Koester, A.; Proynov, E.; St-Amant, A.; Salahub, D. R.; Carravetta, V.; Duarte, H.; Friedrich, C.; Godbout, N.; Guan, J.; Jamorski, C.; Leboeuf, M.; Leetmaa, M.; Nyberg, M.; Patchkovskii, S.; Pedocchi, L.; Sim, F., Triguero, L.; Vela, A. *StoBe-deMon version 3.1*; 2011.
(31) Triguero, L.; Pettersson, L.; Agren, H. *J. Phys. Chem. A* **1998**, *102*, 10599−10607.
(32) Kutzelnigg, W.; Fleischer, U.; Schindler, M. *NMR* **1990**, *23*, 165.
(33) Becke, A. D. *Phys. Rev. A: At., Mol., Opt. Phys.* **1988**, *38*, 3098−3100.
(34) Perdew, J. P.; Yue, W. *Phys. Rev. B: Condens. Matter Mater. Phys.* **1986**, *33*, 8800−8802.
(35) Johnson, R. D. http://cccbdb.nist.gov/, 2015.
(36) Becke, A. D. *J. Chem. Phys.* **1993**, *98*, 5648−5652.
(37) Lee, C.; Yang, W.; Parr, R. G. *Phys. Rev. B: Condens. Matter Mater. Phys.* **1988**, *37*, 785−789.
(38) Nefedov, A.; Wöll, C.; Advanced Applications of NEXAFS Spectroscopy for Functionalized Surfaces. In *Surface Science Techniques*; Bracco, G., Holst, B., Eds.; Springer: Berlin, Heidelberg, 2013; pp 277−303, DOI: 10.1007/978-3-642-34243-1_10.
(39) Wöll, C. *J. Synchrotron Radiat.* **2001**, *8*, 129−135.
(40) Newville, M. *J. Synchrotron Radiat.* **2001**, *8*, 322−324.
(41) Tuinstra, F.; Koenig, J. L. *J. Chem. Phys.* **1970**, *53*, 1126−1130.
(42) Lespade, P.; Al-Jishi, R.; Dresselhaus, M. S. *Carbon* **1982**, *20*, 427−431.
(43) Baghalha, M.; Mohammadi, M.; Ghorbanpour, A. *Fuel Process. Technol.* **2010**, *91*, 714−722.
(44) He, S.; Sun, C.; Yang, X.; Wang, B.; Dai, X.; Bai, Z. *Chem. Eng. J.* **2010**, *163*, 389−394.
(45) Hitchcock, A. P.; Mancini, D. C. *J. Electron Spectrosc. Relat. Phenom.* **1994**, *67*, 1−123.
(46) Atamny, F.; Bloecker, J.; Henschke, B.; Schloegl, R.; Schedel-Niedrig, T.; Keil, M.; Bradshaw, A. M. *J. Phys. Chem.* **1992**, *96*, 4522−4526.
(47) Ade, H.; Urquhart, S. G. In *Chemical Applications of Synchrotron Radiation*; Sham, T. K., Ed.; World Scientific: Singapore, 2002; Advanced Series in Physical Chemistry Vol. *12*.
(48) Kelly, S. D.; Hesterberg, D.; Ravel, B. In *Methods of soil analysis*; Soil Science Society of America: Madison, WI, 2008; Part 5, pp 367−463.
(49) Gago, R.; Jiménez, I.; Albella, J. M. *Surf. Sci.* **2001**, *482*−*485*, 530−536.
(50) Haberstroh, P. R.; Brandes, J. A.; Gélinas, Y.; Dickens, A. F.; Wirick, S.; Cody, G. *Geochim. Cosmochim. Acta* **2006**, *70*, 1483−1494.
(51) Bernard, S.; Beyssac, O.; Benzerara, K.; Findling, N.; Tzvetkov, G.; Brown, G. E., Jr *Carbon* **2010**, *48*, 2506−2516.
(52) Bergmann, U.; Mullins, O. In *Asphaltenes, Heavy Oils, and Petroleomics*; Mullins, O., Sheu, E., Hammami, A., Marshall, A., Eds.; Springer: New York, 2007; pp 139−155.
(53) Clar, E. *Polycyclic Hydrocarbons*; Academic Press: New York, 1964.
(54) Clar, E. *The Aromatic Sextet*; Wiley: New York, 1972.

DOI: 10.1021/acscatal.6b02785
ACS Catal. 2017, 7, 1452−1461